Weierstraß-Institut
für Angewandte Analysis und Stochastik
Leibniz-Institut im Forschungsverbund Berlin e. V.

Preprint ISSN 0946 – 8633

Droplets on liquids and their long way into equilibrium

Stefan Bommer[1], Sebastian Jachalski[2], Dirk Peschka[2],

Ralf Seemann[1,3], Barbara Wagner[2,4]

submitted: March 19, 2013

[1] Experimental Physics
Saarland University
D-66123 Saarbrücken
Germany
E-Mail: stefan.bommer@physik.uni-saarland.de
r.seemann@physik.uni-saarland.de

[2] Weierstrass Institute
Mohrenstr. 39
10117 Berlin
Germany
E-Mail: sebastian.jachalski@wias-berlin.de
dirk.peschka@wias-berlin.de
barbara.wagner@wias-berlin.de

[3] Max Planck Institute for
Dynamics and Self-Organization
37073 Göttingen
Germany

[4] Institute of Mathematics
Technische Universität Berlin
Straße des 17. Juni 136
10623 Berlin
Germany

No. 1773

Berlin 2013

2008 *Physics and Astronomy Classification Scheme.* 68.05.Cf, 02.60.Cb.

Key words and phrases. Liquid-liquid interface structure: measurements and simulations, Numerical simulation, solution of equations .

All authors wish to thank the DFG for financial support through the project *Structure formation in thin liquid-liquid films* in the SPP 1506.

Edited by
Weierstraß-Institut für Angewandte Analysis und Stochastik (WIAS)
Leibniz-Institut im Forschungsverbund Berlin e. V.
Mohrenstraße 39
10117 Berlin
Germany

Fax: +49 30 20372-303
E-Mail: preprint@wias-berlin.de
World Wide Web: http://www.wias-berlin.de/

Abstract

The morphological paths towards equilibrium droplets during the late stages of the dewetting process of a liquid film from a liquid substrate is investigated experimentally and theoretically. As liquids, short chained polystyrene (PS) and polymethyl-methacrylate (PMMA) are used, which can be considered as Newontian liquids well above their glass transition temperatures. Careful imaging of the PS/air interface of the droplets during equilibration by *in situ* scanning force microscopy and the PS/PMMA interface after removal of the PS droplets reveal a surprisingly deep penetration of the PS droplets into the PMMA layer. Droplets of sufficiently small volumes develop the typical lens shape and were used to extract the ratio of the PS/air and PS/PMMA surface tensions and the contact angles by comparison to theoretical exact equilibrium solutions of the liquid/liquid system. Using these results in our dynamical thin-film model we find that before the droplets reach their equilibrium they undergo several intermediate stages each with a well-defined signature in shape. Moreover, the intermediate droplet shapes are independent of the details of the initial configuration, while the time scale they are reached depend strongly on the droplet volume. This is shown by the numerical solutions of the thin-film model and demonstrated by quantitative comparison to experimental results.

1 Introduction

Understanding the dynamics and evolution of patterns in micro- and nanoscale two-layer immiscible thin films is of fundamental importance for the design of functional surfaces for numerous applications ranging from model for tear film of the human eye [1] to instabilities during the fabrication of polymer/polymer solar cells [2]. The past decades has seen many investigations of such systems, both experimentally and theoretically. But besides of its technological relevance and its scientific interest, the in-depth understanding of these processes is still superficial compared to liquid dewetting from solid substrates and quantitative experimental verification is still missing. For experimental reasons the morphology and the dynamics of liquid/liquid dewetting was typically studied using polymers as high molecular liquids. For the model two-layer system of polystyrene (PS) on polymethyl-methacrylate (PMMA), the shape of an underlying liquid (PMMA) and the liquid polystyrene (PS) rim profile dewetting from this substrate has been studied experimentally in the pioneering work of the group of G. Krausch [3, 4]. As a result, they found a characteristic shape and dewetting dynamics, depending on the relative viscosity of the two liquids. The experimentally observed behavior was claimed to be in agreement with another important work by Brochard-Wyart et al. [5]. However, this is surprising since the dewetting velocity strongly depends on film thickness and which are not considered in [5]. However, the used polymers in [3, 4] are above the entanglement of the respective chain length and viscoelastic properties cannot be ruled out in this system. Other groups studied the breakup and the hole growth of a liquid-liquid system where the viscosity of one of the liquids is much larger than the viscosity of the other liquid [6] and in the special case, where the resulting dewetting morphologies are coated with a thin layer of the underlying liquid [7], whereas the characteristic shape of the liquid-liquid interface was not explored in detail. Similar results on dewetting rim shapes can be found also in [6, 8–12] for different polymer-polymer dewetting systems. However, in none of those experimental studies the parameters are worked out well enough to allow for a quantitative comparison with theoretical results. While many of the theoretical works have focussed on linear stability analysis and numerical simulations of short time and long-time evolution [13, 14], Golovin and Fisher [14, 15] even in the presence of surfactant [16], a systematic comparison to experimental results for the simplest possible system will be important to build a fundamental understanding of this system.

In this study we present a quantitative comparison of experimentally obtained transient and equilibrium drop shapes to numerically and analytically drop shapes for a model system using short-chained PS/PMMA, that can be described via a Stokes model for the multiphase flow of two immiscible liquids with capillary boundaries and driven by the intermolecular forces between the liquids. In our experiments we obtain 3d dynamic and equilibrium droplets shapes by following the complete dewetting process. The relevant parameters required for the comparison with theoretical derived dynamic droplet shapes, *i.e.* the surface tension ratio and the contact angle, are obtained by comparing the experimental equilibrium droplet shapes to the exactly know theoretical shapes. These values are used as input parameters in our dynamic thin-film model to compare the various morphological transitions long before reaching equilibrium. Except for a short initial phase the morphology was found to be independent on the initial start conditions. This independence of the transient droplet shapes allows for quantitative comparison of the experimentally determined drop morphologies to the theoretically droplet shapes calculated using the experimentally determined input parameters.

2 Methods

For our liquid/liquid experiments we prepared thin polystyrene (PS) films on top of underlying polymethyl-methacrylate (PMMA) films which are supported by silicon wafers: Silicon rectangles of about $2\,\mathrm{cm}^2$ were cut from 5"-wafers with $\langle 100 \rangle$ orientation. The pieces were pre-cleaned by a fast CO_2-stream (snow-jet, Tectra) and sonicated in ethanol, acetone and toluene followed by a bath in peroxymonosulfuric acid and a careful rinse with Millipore$^{\mathrm{TM}}$ water. On top of the cleaned silicon wafers, PMMA films were spun from toluene solution with thicknesses ranging from $80\,\mathrm{nm}$ to $700\,\mathrm{nm}$. The dewetting PS films cannot be spun directly on top of the PMMA with the desired thickness anleft=3cm,right=3cm,top=3cm,bottom=3cmd were, in a first step, spun from toluene solution onto freshly cleaved mica sheets with thicknesses ranging from $7\,\mathrm{nm}$ to $22\,\mathrm{nm}$. In a second step, the glassy PS films were transferred onto a water surface (Millipore$^{\mathrm{TM}}$) and picked up with the PMMA coated silicon substrates.

Both polymers were purchased from Polymer Standard Service Mainz (PSS-Mainz, Germany) with $M_w/M_n = 1.03$ and molecular weights of $M_w = 9.6\,\mathrm{kg/\,mol}$ for PS and $M_w = 9.9\,\mathrm{kg/\,mol}$ in case PMMA. The molecular weights are well below the entanglement lengths of PS and PMMA and their melts can be treated as Newtonian liquids [17–21] at temper-

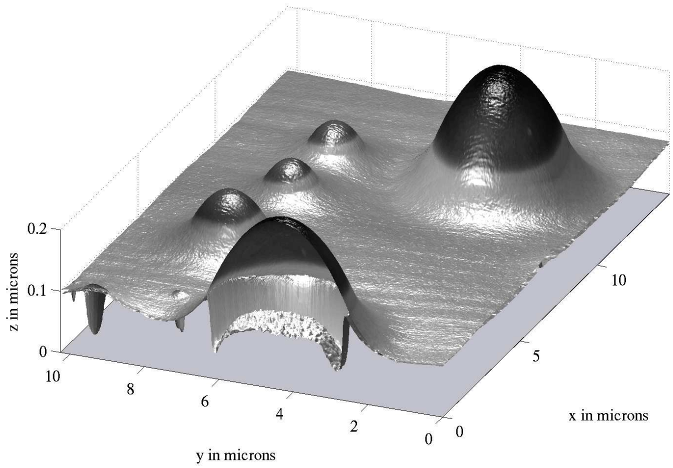

Figure 1: Composition of AFM top and bottom topographies after dewetting at $T = 140$ °C for $45\,\mathrm{min}.$ Initial top layer thickness $80\,\mathrm{nm}$ PMMA and bottom layer thickness $20\,\mathrm{nm}$ PS layer lead to isolated droplets, which are not yet in equilibrium

atures above their bulk glass transition temperatures T_G of about $T_{\text{G,PS}} = 85 \pm 5$ °C and $T_{\text{G,PMMA}} = 115 \pm 5$ °C for PS and PMMA, respectively. The glassy sample can be stored in the lab at room temperature and the liquid/liquid dewetting process is started when heating the sample above the glass transition temperature of the polymers. The dewetting experiments were typically conducted at a temperature of $T = 140$ °C resulting in viscosities of $\mu_{\text{PS}} \approx 2\,k\mathrm{Pa\,s}$ for the dewetting PS and $\mu_{\text{PMMA}} = 675\,k\mathrm{Pa\,s}$ for the underlying PMMA film. The viscosity values were extracted from [22, 23].

The dewetting process was monitored *in situ* at 140 °C by atomic force microscopy (AFM) in Fastscan Mode$^{\text{TM}}$ (Bruker, Germany). To determine additionally the shape of the liquid PS /PMMA interface the dewetting process is stopped at a desired dewetting stage by quenching the sample temperature from $T = 140$ °C to room temperature. At this temperature both polymers are glassy and the sample can be easily stored and handled. The glassy PS structures are removed by a selective solvent (cyclohexane, Sigma Aldrich, Germany) and the remaining PMMA surface with the shape of the formerly PS/PMMA interface frozen into it is subsequently imaged by AFM. The full three dimensional shape of the dewetting PS structures are obtained by combining the surfaces of the related topographies as determined by AFM as shown in fig. 1.

3 Results and discussion

3.1 Equilibrium droplets

In this section we aim to characterize the subsequently used Si/PMMA/PS/air system by its equilibrium configuration, *i.e.* liquid PS lenses swimming on liquid PMMA supported by silicon. We

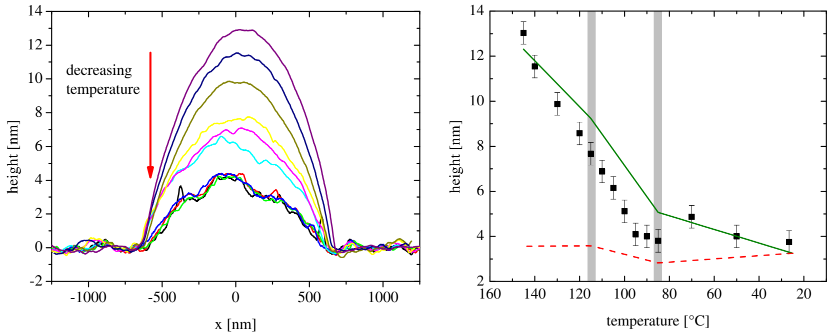

Figure 2: (left) Cross sections of the same polystyrene droplet imaged *in situ* by AFM while cooling the sample from 145 °C to 30 °C. The entire duration of this cooling cycle was about 70 minutes. (right) Temperature dependent height of the droplet as obtained from AFM data with glass transition temperatures of PS and PMMA are indicated. The solid line shows the expected height change based on thermal expansion polymers when assuming a constant width of the droplet. The dashed line denotes a similar model calculating assuming just the linear expansion coefficients.

will first discuss the experimental method to measure droplet shapes, give explicit expressions for equilibrium states and describe how surface tension values can be extracted from those and finally compute contact angles.

In previous experiments no change of the dewetting profile could be detected when cooling and freezing a polystyrene dewetting structure on a solid substrate, *e.g.* [17]. However, in our liquid/liquid system it was found that the PS/air interfaces significantly change their shape upon cooling. A PS droplet that raised out of the PMMA by *e.g.* 12 nm at $T = 140$ °C just raises out of the PMMA by 1-2 nm at room temperature. And as we aim at a quantitative comparison with theoretical results it is of utmost importance to clarify the origin of the shape change and to develop a suitable experimental protocol.

To observe the shape change of the PS/air interface during a temperature change, the PS/air interfaces of several droplets were measured while cooling and heating. As a first result, the shape change during heating and cooling cycles turned out to be reversible, see fig. 2 for a cooling cycle. Considering the viscosities of both polymers as well as the experimentally found independence of the droplet shape from the cooling/heating rate (tested from milliseconds to hours), a lateral equilibration *e.g.* according to temperature dependent surface tensions is not expected. This could be confirmed experimentally as no dependence of the in-plane radius of the droplet with temperature could be detected within an experimental error of about $\pm 10\,\mathrm{nm}$. However, the height of the droplet changes significantly showing a characteristic step in the shape change as function of temperature, see fig. 2

Even not knowing the thermal expansion coefficients precisely, as slightly different values can be found in literature, the height change of the droplet can be explained by simple model assumptions. The approximate thermal volume expansion coefficients of PS are $\alpha_{\mathrm{PS,T<T_G}} \approx 2 \cdot 10^{-4}$, $\alpha_{\mathrm{PS,T>T_G}} \approx 5.5 \cdot 10^{-4}$ and for PMMA $\alpha_{\mathrm{PMMA,T<T_G}} \approx 2.7 \cdot 10^{-4}$, $\alpha_{\mathrm{PMMA,T>T_G}} = 5.4 \cdot 10^{-4}$ [24]. The remarkably change of expansion coefficient at the glass transition temperature is char-

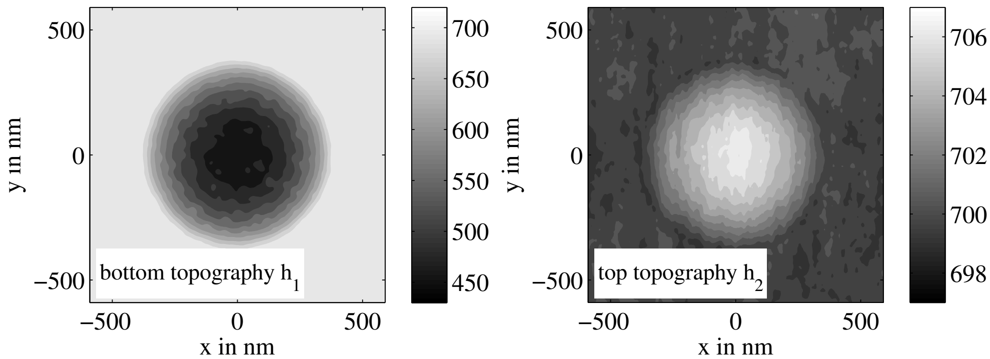

Figure 3: Measured equilibrium drop profile as determined by AFM. The height scales in nanometers are shown to the right of each panel. (*left*) bottom profile h_1 and (*right*) top profile h_2.

acteristic for polymers: At room temperature both polymers are glassy whereas the E module of the PMMA is larger than that of PS. Accordingly the shape of the PS/PMMA interface is expected to remain constant during the temperature increase and the entire thermal volume expansion of the PS is used to increase the height of the droplet. Reaching the glass transition temperature of PS, the PS expands almost three times faster with temperature, *i.e.* twice as fast as the still glassy PMMA. This change in thermal expansion coefficient thus explains the pronounced step in the droplet height for temperatures $T > T_{\mathrm{G,PS}}$. When reaching the glass transition temperature of PMMA, the expansion ratios of both polymers are again similar. Still assuming that no lateral equilibration of the lower droplet shape occurs, the height change of droplet with temperature is just slightly reduced as we still expect the difference between the linear expansion for PMMA and the volume expansion of PS, see solid line in fig. 2 (right panel). Repeating the same reasoning assuming an isotropic change in droplet volume we have to calculate the height change of the droplet based on the linear expansion coefficients of both polymers which are three times smaller than the corresponding volume expansion coefficients. The result of this model calculation is plotted as dashed line in fig. 2 (right panel). Comparing the result of both model calculations to the experimental data we can conclude that the height change of the droplets results in fact from the thermal expansion of the polymers while the PS/PMMA interface remains about constant during this temperature induced shape change.

Based on this result we validated our experimental protocol to obtain quantitative drop shapes: The top side of the droplets, *i.e.* the PS/air interface is imaged at the applied dewetting temperature and combined with the PMMA/PS interface measured at room temperature after removing the PS structure.

Extraction of surface tension and contact angles

Using the measured three dimensional PS drop profiles we will derive the contact angles and the ratios of the surface tensions from their equilibrium shapes. These values will serve as input parameters for the computed drop morphologies and could not be found in literature with the needed precision [25, 26]. The analysis of the experimental equilibrium drop shapes is based

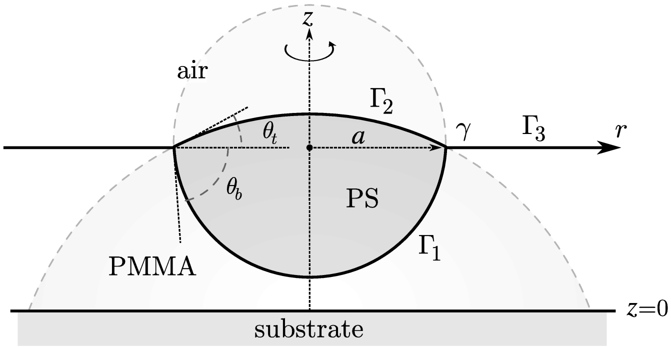

Figure 4: Sketch of a axisymmetric liquid lens in equilibrium with $\Gamma_1, \Gamma_2, \Gamma_3$ being the PS/PMMA, PS/air, PMMA/air interface respectively and γ the triple-junction. Each interface Γ_i has the surface tension σ_i. The radius of the lens is a and the contact angles are θ_t, θ_b (top, bottom). Furthermore for planar axisymmetric droplets we have $\mathbf{n}_{\Gamma_1} = -\mathbf{e}_r \cos\theta_b - \mathbf{e}_z \sin\theta_b$, $\mathbf{n}_{\Gamma_2} = -\mathbf{e}_r \cos\theta_t + \mathbf{e}_z \sin\theta_t$, $\mathbf{n}_{\Gamma_3} = \mathbf{e}_r$.

on the following reasoning: Liquid equilibrium droplets with constant surface-tension $\sigma_\alpha > 0$ deform an underlying liquid substrate to minimize the surface energy

$$E = \sum_{\alpha=\{1,2,3\}} \sigma_\alpha \int_{\Gamma_\alpha} d\Gamma, \tag{1}$$

where $\alpha = 1, 2, 3$ corresponds to the surface tensions of the PS/PMMA, PS/air, and PMMA/air interface as indicated in fig. 4. The minimization is understood with respect to all deformations of the liquid domains (PS and PMMA) for which the total volumes are fixed. The resulting variation with velocity field $\mathbf{u}$ is given by

$$\begin{aligned} \delta E[\mathbf{u}] = &\sum_\alpha \sigma_\alpha \left(\int_\gamma \mathbf{u}\cdot\mathbf{n}_{\Gamma_\alpha} \mathrm{d}\gamma - \int_{\Gamma_\alpha} 2H_\alpha \mathbf{u}\cdot\mathbf{n}\, d\Gamma \right) \\ &+ \int_{\Gamma_1\cup\Gamma_3} \Lambda_1 \mathbf{u}\cdot\mathbf{n} d\Gamma + \int_{\Gamma_1\cup\Gamma_2} \Lambda_2 \mathbf{u}\cdot\mathbf{n} d\Gamma \end{aligned} \tag{2}$$

where Λ_1, Λ_2 are the Lagrange multipliers associated with volume conservation. This leads to the Neumann-triangle, a local condition stating that contact angles fulfill

$$\sum_{\alpha=\{1,2,3\}} \sigma_\alpha \mathbf{n}_{\Gamma_\alpha} = 0, \tag{3}$$

and each interface Γ_α has constant mean curvature H_α. The normalized vector $\mathbf{n}_\alpha$ is tangential to the corresponding interface Γ_α and normal to the contact line γ as also indicated in fig. 4.

Introducing the spreading coefficient $\sigma = \sigma_3 - \sigma_1 - \sigma_2$ one can easily verify that equilibrium droplets as in (3) only exist if $(-\sigma) > 0$ and $\sigma_1, \sigma_2 > \frac{1}{2}(-\sigma)$. A sketch of the equilibrium configuration is shown in fig. 4. From a measured equilibrium configuration we can thus extract the values for surface tension as follows: If for instance σ_3 is given, then one can determine the other two surface tensions from the contact angles by solving the linear equation

$$\begin{pmatrix} \cos\theta_t & \cos\theta_b \\ -\sin\theta_t & \sin\theta_b \end{pmatrix} \begin{pmatrix} \sigma_2 \\ \sigma_1 \end{pmatrix} = \begin{pmatrix} \sigma_3 \\ 0 \end{pmatrix} \tag{4}$$

where $\theta_t, \theta_b > 0$ are measured. For contact angles $\theta_t, \theta_b \leq 90°$ a liquid lens has the following equilibrium shape for $r \leq a$

$$h_2(x,y) = h_\infty + \left(\sqrt{H_2^{-2} - r^2} - \sqrt{H_2^{-2} - a^2}\right) \tag{5a}$$

$$h_1(x,y) = h_\infty - \left(\sqrt{H_1^{-2} - r^2} - \sqrt{H_1^{-2} - a^2}\right) \tag{5b}$$

and $h_1(x,y) = h_2(x,y) = h_\infty$ for $r > a$. We use the radial coordinate $r^2 = (x - x_0)^2 + (y - y_0)^2$ and call a the radius of the droplet. We used the standard representation of interfaces Γ_i by graphs of functions, *i.e.*

$$\Gamma_1 = \{(x,y,z) \in \mathbb{R}^3 : z = h_1(x,y), 0 < h_1 < h_2\}, \tag{6a}$$

$$\Gamma_2 = \{(x,y,z) \in \mathbb{R}^3 : z = h_2(x,y), 0 < h_1 < h_2\}, \tag{6b}$$

$$\Gamma_3 = \{(x,y,z) \in \mathbb{R}^3 : z = h_1(x,y), 0 < h_1 = h_2\}. \tag{6c}$$

Note that up to an additive constant basically $h_1(x,y)$ and $h_2(x,y)$ are the morphologies measured by the AFM, where h_2 is measured at $T = 140$ °C and h_1 after the removal of the PS by an selective solvent.

A least-squares fit of (5) to the measured AFM topography data returns the six parameters h_∞, H_1, H_2, a, x_0 and y_0. Since both interfaces, *i.e.* h_1 and h_2 are measured independently and the AFM can only measure height differences, h_∞, x_0, y_0 have no absolute value, so one might define $x_0 = y_0 = 0$ and h_∞ as the values set by the preparation of the PMMA layer and as determined independently. Also h_2 is measured in its liquid state and h_1 after solidification and removal of the PS by a selective solvent. Using the values for H_α and a the contact angles can be directly computed via

$$\theta_b = \arctan\left(a/\sqrt{H_1^{-2} - a^2}\right), \tag{7a}$$

$$\theta_t = \arctan\left(a/\sqrt{H_2^{-2} - a^2}\right). \tag{7b}$$

Inserting this into (4) gives the surface tensions.

Fitting spherical caps (5) to the top and bottom profiles of several droplets, see fig. 5, we obtain a relationship between a_t, a_b and H_1, H_2, respectively which is shown in fig. 6. For constant contact angles (7) suggests that the relationship between curvature and radius must be linear which agrees within the experimental accuracy with the experimental data.

Note that due to the magnitude of systematic and statistical errors no evidence for a deviation from a linear relation in fig. 6 could be observed.

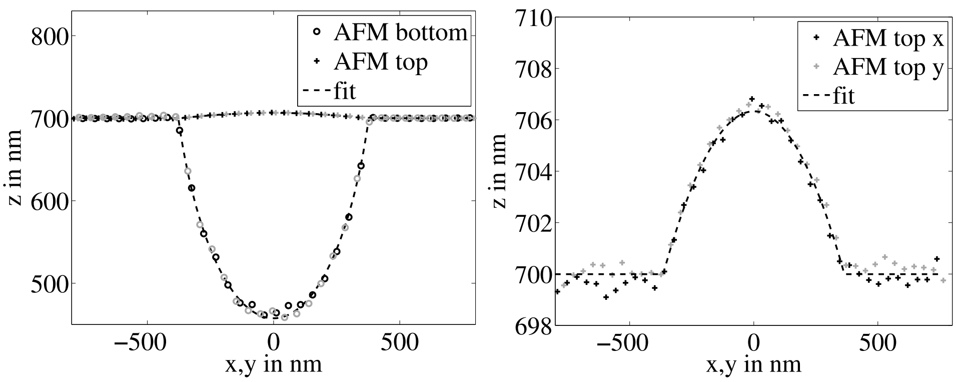

Figure 5: (*left*) Top and bottom AFM topography of an equilibrium droplet. Two cross sections cut perpendicular through the droplet in x-direction (dark symbols) and y-direction (light symbols) are shown together with the fit using eq. (5) (dashed line); (*right*) close-up of the top AFM topography including fit function.

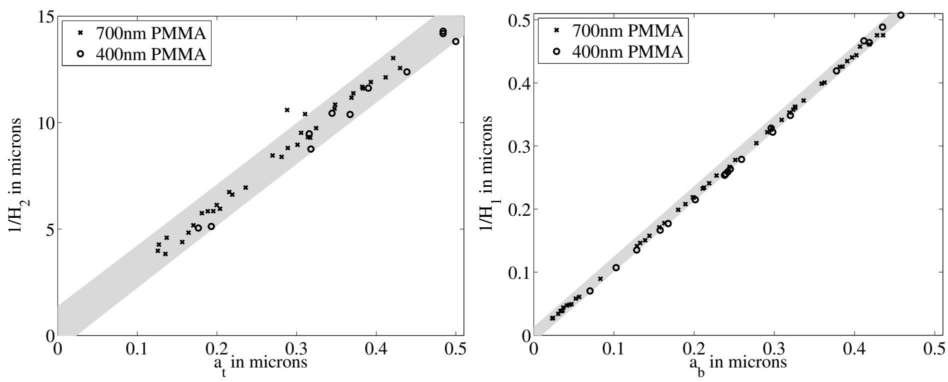

Figure 6: (top) Curvature of the top spherical caps and (bottom) curvature of bottom spherical caps as a function of droplet radius a measured from equilibrium droplets on $400\,\mathrm{nm}$ thick PMMA substrates (circles) and $700\,\mathrm{nm}$ thick PMMA substrates (crosses) with linear fit (shaded area 95% confidence interval) gives $H_1^{-1} = (1.11 \pm 0.02)a_b$ and $H_2^{-1} = (29 \pm 1)a_t$ and corresponding contact angles $\theta_b = (64 \pm 2)^\circ$ and $\theta_t = (1.98 \pm 0.07)^\circ$.

From the linear relationship between radius and curvature shown in fig. 6 and using (7) we obtain for the top angle $\theta_\mathrm{t} \approx (1.98 \pm 0.07)°$ and for the bottom angle $\theta_\mathrm{b} \approx (64 \pm 2)°$ where the error is composed from the statistical error in the fit and the systematic error in the determination of the droplet radius. Using (4) we obtain the surface tensions of the PS/PMMA interfaces

$$\sigma_1 = (0.038 \pm 0.002)\sigma_3 = (1.22 \pm 0.07)\, m\mathrm{N}/\,\mathrm{m},$$

and of the PS/air interface

$$\sigma_2 = (0.984 \pm 0.001)\sigma_3 = (31.49 \pm 0.03)\, m\mathrm{N}/\,\mathrm{m},$$

based on the PMMA/air surface tension $\sigma_3 = 32\,\mathrm{mN}/\,\mathrm{m}$ at $T = 140$ °C taken from [26]. The corresponding spreading coefficient is $\sigma = (-0.022 \pm 0.003)\sigma_3 = (-0.7 \pm 0.1)\,\mathrm{mN}/\,\mathrm{m}.$

3.2 Nonequilibrium droplet shapes

Now we are using the parameters extracted from the equilibrium droplet shapes in order to plug them into a thin-film model and to investigate the evolution of droplets near equilibrium. Therefore we shortly explain how such a model is derived from a free boundary problem and how the corresponding partial differential equation is discretized using the method of finite differences. The question of fidelity of the lubrication approximation for the particular combination of surface tensions is beyond the scope of this paper and will be investigated in future. Since it is quite unrealistic that we can obtain sufficiently precise initial data from the experiment and use these for a numerical simulation, we first check the dependence of our results on a particular choice of initial data. Then we compare a set of simulations for a fixed initial PMMA layer thickness of $80\,\mathrm{nm}$ at a specific time with corresponding experiments at exactly the same physical time.

Let us consider the final evolution of PS droplets on PMMA as they approach their stationary state. The Stokes equation which describes the evolution of the free boundaries $\Gamma_1(t), \Gamma_2(t)$, $\Gamma_3(t)$ by a velocity $\mathbf{u}$ or correspondingly the evolution of $h_1(t,x,y)$ and $h_2(t,x,y)$ has a dissipative structure with energy E in (1) and for Newtonian liquids the dissipation

$$D = \sum_{i=1}^{2} \int_{\Omega_i} \frac{\mu_i}{2} (\nabla \mathbf{u} + \nabla \mathbf{u}^\top)^2 \, dx\, dy\, dz.$$

After a standard lubrication approximation, where one assumes that the interfaces are shallow $\|\nabla h_1\|^2, \|\nabla h_2\|^2 = \mathcal{O}(\varepsilon^2)$ for $\varepsilon \ll 1$ a formal asymptotic calculation shows that $h_1(t,x,y)$, $h_2(t,x,y)$ are solutions of a fourth-order, degenerate parabolic equation. A standard method to circumvent the degeneracy of that equation and to avoid the non-smoothness of the energies is to introduce a precursor using an energy

$$E_{h_*} = \int \left[\tfrac{1}{2} \tfrac{\sigma_1}{\sigma_2} \|\nabla h_1\|^2 + \tfrac{1}{2} \|\nabla h_2\|^2 + V_{h_*} \right] \, dx\, dy. \tag{8}$$

where $V_{h_*} = V_{h_*}(h_2 - h_1)$ also has the interpretation of an intermolecular potential which encodes van-der-Waals interactions and the appropriate Neumann contact angle.

This leads to the following system of degenerate parabolic equations

$$\partial_t h_i = \sum_{j=1}^{2} \nabla \cdot \left(Q_{ij}\, \nabla \pi_j \right), \qquad\qquad i = \{1,\, 2\}, \tag{9a}$$

where divergence and gradient are component-wise and with mobility matrix

$$Q = \frac{1}{\mu} \begin{pmatrix} \frac{1}{3}h_1^3 & \frac{1}{2}h_1^2(h_2 - \frac{1}{3}h_1) \\ \frac{1}{2}h_1^2(h_2 - \frac{1}{3}h_1) & \frac{1}{3}(\mu - 1)(h_2 - h_1)^3 + \frac{1}{3}h_2^3 \end{pmatrix} \tag{9b}$$

and $\mu = \mu_1/\mu_2$ is the ratio of PMMA to PS viscosity. The reduced pressures are defined $\pi_j = \delta E_{h_*}/\delta h_j$. This expansion is only valid if $\varepsilon = \sqrt{(-\sigma)/\sigma_2} \ll 1$. All quantities above are non-dimensional and scaled using

$$[z] = H, \qquad [x] = [y] = \varepsilon^{-1} H, \qquad [t] = \varepsilon^{-4} H \frac{\mu_2}{\sigma_2}$$

for some height scale $H = 20\,\mathrm{nm}$ which we define in correspondence to the initial PS layer thickness. Using the values of the surface tension and known viscosities mentioned in the methods section we obtain $\varepsilon = 0.15$, $[x] = 133\,\mathrm{nm}$, $[t] = 2.1\,\mathrm{sec}$, $\mu = 350$ and $\sigma_1/\sigma_2 = 0.039$. Note that in [27] some of the authors studied stationary solutions of (9) and highlighted the connection between E in (1) and E_{h_*} in (8) as an appropriate limiting problem for shallow interfaces and as $h_* \to 0$.

For better readability we state the model in non-dimensional form but all results, *e.g.* numerical solutions, are presented in dimensional form again. The particular potential we use is $V_{h_*}(h) = 2h_*^3/h^3 - 3h_*^2/h^2$ and typically we use $h_* = 1/64$. Note that with such a small h_* it is only important that V_{h_*} assumes its unique minimum $V_{h_*}(h_*) = -1$ and $V_{h_*} \nearrow 0$ as $h \gg h_*$ and $0 < h_* \ll 1$. Furthermore our particular V_{h_*} satisfies $V_{h_*} \to \infty$ as $h \to 0$. With larger h_* instabilities and effects related to *e.g.* spinodal dewetting will become more important. Note that for the model reduction to be asymptotically correct we need $(-\sigma) = O(\varepsilon^2)$ but $\sigma_1, \sigma_2, \sigma_3 = O(1)$. As we showed in the previous section we have $0 < (-\sigma) \ll \sigma_2$ but $(-\sigma) \sim \sigma_1$. Nevertheless, we observed, by comparison to preliminary calculations based on the full Stokes model that the lubrication approximation still yields quite accurate results. In fact, for many similar thin-film problems, see *e.g.* [28] or [29] lubrication approximation is still useful near or even beyond its formal validity.

In order to solve the axisymmetric system of lubrication equations (9) we use a finite difference scheme with spatial and temporal adaptivity. The spatial adaptivity is of second order and heuristically adds points near the would-be triple junction, where second derivatives become large as $h_* \to 0$. The time discretization uses a fully implicit Euler method and the temporal adaptivity is achieved with standard step-size bisection to control the error. With the exception of interpolation during a mesh adaptation the scheme conserves the mass $m_i = 2\pi \int_0^R h_i(t,r) r\, dr$. Boundary conditions at $r = R$ and $r = 0$ are Neumann conditions for h_i and π_i. As initial data for our comparison we use

$$h_1(t=0, r) = 4H, \tag{10a}$$

$$h_2(t=0, r) = \begin{cases} 4H + Hh_* + h & r < r_0 \\ 4H + Hh_* & r \geq r_0 \end{cases} \tag{10b}$$

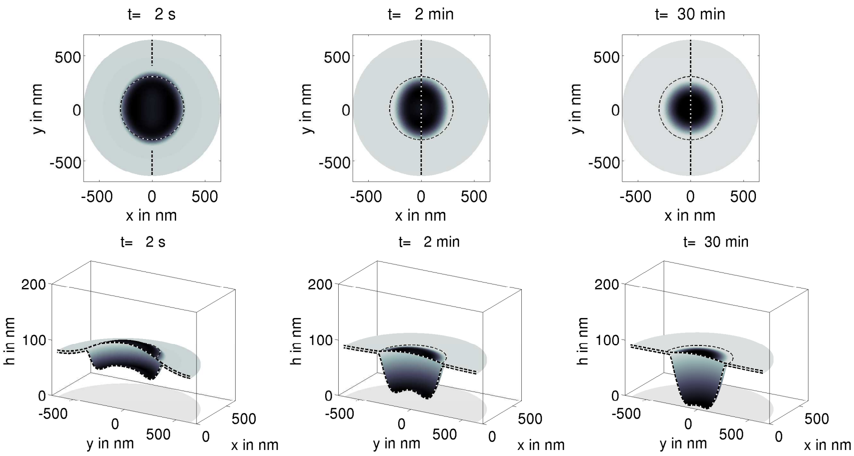

Figure 7: Numerical solutions of the $2d$ thin-film equation with nonsymmetric initial data and $h_* = 1/5$ and other parameters as before at $t = 2\,\mathrm{sec}, 2\,\mathrm{min}, 30\,\mathrm{min}$ (*top*) top view (*bottom*) 3d view showing a quick evolution into a nearly axisymmtric state followed by an evolution where $h_1 \to 0$.

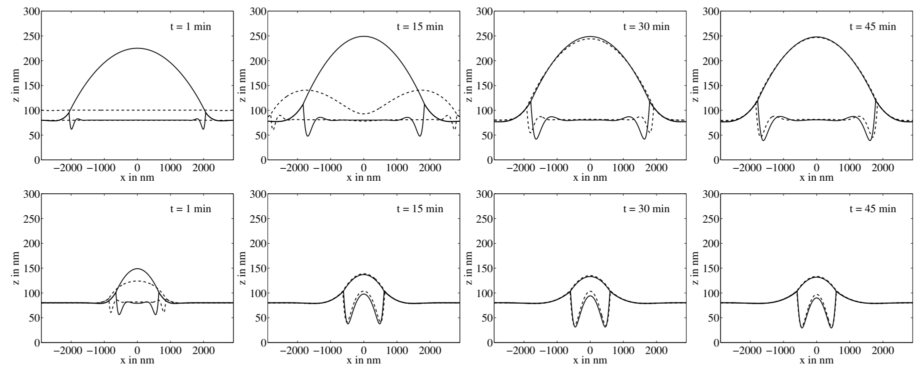

Figure 8: Numerical simulation of droplet formation and equilibration for two PS volumes and different initial configurations at different times. (top) $r_0 = 32L, h = H$ and $r_0 = 16L, h = 4H$ and (bottom) $r_0 = 8L$, $h = H$ and $r_0 = 4L$, $h = 4H$ ($H = 20\,\mathrm{nm}, L = 133\,\mathrm{nm}$)

where the initial disc radii r_0 and heights h are choosen to match the volumes and layer thickness prepared in the experiments.

Now we consider numerical solutions of the thin film equation and their evolution towards equilibrium. In particular we fist show numerical solutions with two different volumes $2\pi \int (h_2 - h_1) r\, dr = \{1.14, 0.07\}\,\mu\mathrm{m}^3$. For each volume we use two different initial configurations as in (10). The strong volume dependence of the approach to equilibrium is demonstrated in fig. 8, where a synchronization of the different solutions can be observed as time progresses to infinity.

For the biggest droplet in the first row of fig. 8 this happens only after $45\,\mathrm{min}$, while for the smallest droplets in the lower row different initial data are synchronized after less than $1\,\mathrm{min}$. In our numerical simulations we have also started with asymmetric initial shapes and observe a quick approach to symmetrical shapes before the intermediate stages towards equilibrium have begun, see for illustration fig. 7

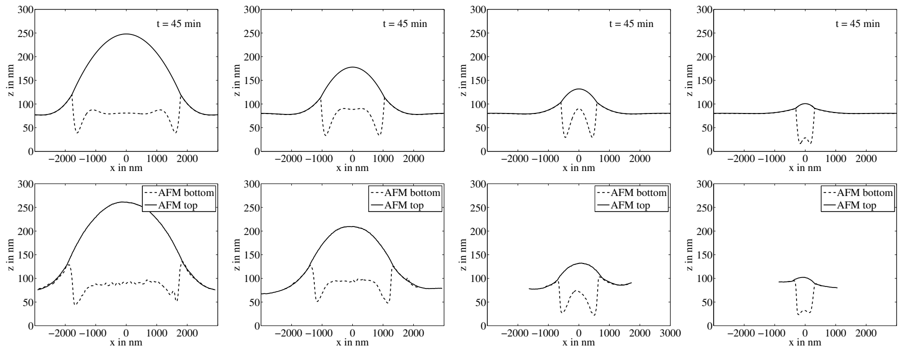

Figure 9: PS$(10k)$ droplets on PMMA$(10k)$ substrates at $T = 140$ °C after dewetting a sample for $t = 45\,\mathrm{min}$. The initially flat PMMA and PS layers had a thickness of $h_1 = 80\,\mathrm{nm}$ and $h_2 - h_1 = 20\,\mathrm{nm}$, respectively. (*upper column*) simulations and (*lower column*) AFM measurements of similar volumes.

Experiments vs thin-film model

Using the precise knowledge of the surface tensions of our system and the weak dependence on initial data we are now able to follow the complete dewetting process to understand the stages of equilibration of a droplet by comparing these stages in experiment and simulation. For a given measurement at a certain time there is an upper bound in droplet size above which droplets are not axisymmetric with their shape strongly dependent on initial data. In practice this implies that for the used liquid/liquid system of PS$(10k)$ and PMMA$(10k)$ at $T = 140$ °C and realistic experimental time scales of a few days we are limited to droplets of a few micrometers in radius. For experimental reason, as explained in the methods section, it is not possible to follow the liquid-liquid interface of a single droplet on its way to equilibrium. Thus different droplet volumes were imaged at the same dewetting time and compared to the related simulations.

Figure 9 shows this comparison just just after having reached the time where the drop shapes are become independent from the initial configuration. The experimental data compare quite well with the numerical solution of our lubrication model for all examined volumes verifying the extracted knowledge from the equilibrium droplets. Also for the late stages of the experiment shown in fig. 10 this proves to be true.

The remaining differences between simulation and experiment for larger times are suspected due be caused by possible slip effects at the substrate/PMMA interface, or intermolecular forces between the substrate and PMMA, which we so far have neglected in our model. This will be subject of our future investigations.

4 Conclusion

In this paper we considered the slow evolution of liquid PS droplets on liquid PMMA substrate into equilibrium. We extracted surface tensions from equilibrium morphologies, which was necessary for two reasons: Firstly, the values found in literature depend on temperature and molec-

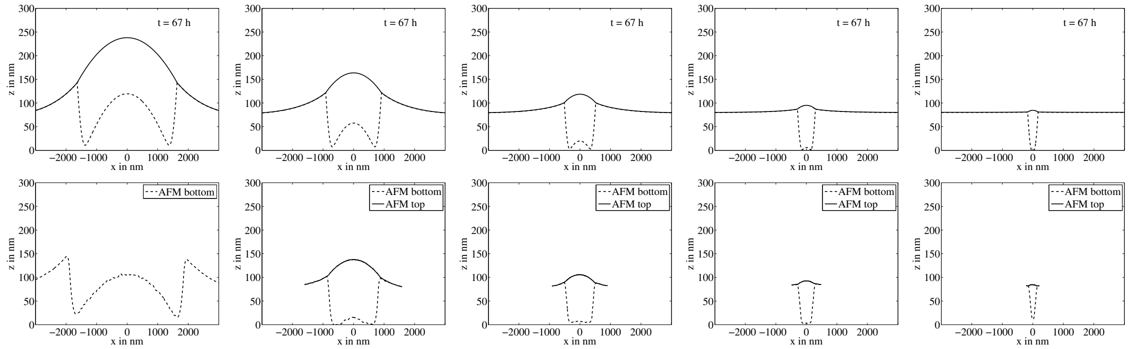

Figure 10: PS($10k$) droplets on PMMA($10k$) substrates at $T = 140$ °C after dewetting a sample for $t = 67\,\mathrm{h}$. The initially flat PMMA and PS layers had a thickness of $h_1 = 80\,\mathrm{nm}$ and $h_2 - h_1 = 20\,\mathrm{nm}$, respectively. (*upper column*) simulations and (*lower column*) AFM measurements of similar volumes.

ular weight, whereas the parameter regimes studied in literature do not overlap with ours, *i.e.* $T = 140$ °C and $M_w \approx 10\,\mathrm{kg/\,mol}$ for PS and PMMA. Secondly, the sign of the spreading coefficient depends sensitively on the precise value of the surface tensions and is crucial for quantitative comparison.

The surface tension data obtained by this precise validation experiment is then used to compare experimentally measured surface/interface profiles with the ones obtained by numerically solving a thin-film equation for liquid two-layer films. Since the numerical solutions only depend on initial data through the total drop volume, we performed quantitative comparisons and found very good agreement for droplet shapes at similar times and drop volumes.

References

[1] Y. L. Zhang, O.K. Matar, and R.V. Craster. Analysis of tearfilm rupture: effect of non-Newtonian rheology. *J. Coll. Int. Sci.*, 262:130–148, 2003.

[2] Y. L. Zhang, O.K. Matar, and R.V. Craster. An interfacial instability in a transient wetting layer leads to lateral phase separation in thin spin-cast polymer-blend films. *Nature Materials*, 4:782–786, 2005.

[3] P. Lambooy, K.C. Phelan, O. Haugg, and G. Krausch. Dewetting at the liquid-liquid interface. *Physical Review Letters*, 76(7):1110–1113, 1996.

[4] C. Wang, G. Krausch, and M. Geoghegan. Dewetting at a polymer-polymer interface: film thickness dependence. *Langmuir*, 17(20):6269–6274, 2001.

[5] F. Brochard Wyart, P. Martin, and C. Redon. Liquid/liquid dewetting. *Langmuir*, 9(12): 3682–3690, 1993.

[6] R.A. Segalman and P.F. Green. Dynamics of rims and the onset of spinodal dewetting at liquid/liquid interfaces. *Macromolecules*, 32(3):801–807, 1999.

[7] D. Slep, J. Asselta, M. H. Rafailovich, J. Sokolov, D.A. Winesett, A.P. Smith, H. Ade, and S. Anders. Effect of an Interactive Surface on the Equilibrium Contact Angles in Bilayer Polymer Films. *Langmuir*, 16:2369–2375, 2000.

[8] Q. Pan, K.I. Winey, H.H. Hu, and R.J. Composto. Unstable polymer bilayers. 2. the effect of film thickness. *Langmuir*, 13(6):1758–1766, 1997.

[9] Y. Li, Y. Yang, F. Yu, and L. Dong. Surface and interface morphology of polystyrene/poly (methyl methacrylate) thin-film blends and bilayers. *Journal of Polymer Science Part B: Polymer Physics*, 44(1):9–21, 2005.

[10] C. Neto. A novel approach to the micropatterning of proteins using dewetting of polymer bilayers. *Phys. Chem. Chem. Phys.*, 9(1):149–155, 2006.

[11] A. M. Higginsa, M. Sferrazza, R. A. L. Jones, P.C. Jukes, J.S. Sharp, L. E. Dryden, and J. Webster. The timescale of spinodal dewetting at a polymer/polymer interface. *Eur. Phys. J. E*, 8:137–143, 2002.

[12] J.P. de Silva, M. Geoghegan, A.M. Higgins, G. Krausch, M.O. David, and G. Reiter. Switching layer stability in a polymer bilayer by thickness variation. *PRL*, 98(26):267802, 2007.

[13] A. Pototsky, M. Bestehorn, D. Merkt, and U. Thiele. Morphology changes in the evolution of liquid two-layer films. *The Journal of Chemical Physics*, 122(22):224711, 2005.

[14] L.S. Fisher and A.A. Golovin. Nonlinear stability analysis of a two-layer thin liquid film: Dewetting and autophobic behavior. *Journal of colloid and interface science*, 291(2):515–528, 2005.

[15] D. Bandyopadhyay, R. Gulabani, and A. Sharma. Instability and dynamics of thin liquid bilayers. *Ind. Eng. Chem. Res*, 44(5):1259–1272, 2005.

[16] L.S. Fisher and A.A. Golovin. Instability of a two-layer thin liquid film with surfactants: Dewetting waves. *Journal of colloid and interface science*, 307(1):203–214, 2007.

[17] R. Seemann, S. Herminghaus, and K. Jacobs. Shape of a liquid front upon dewetting. *Physical Review Letters*, 87(19):196101, 2001.

[18] J. Becker, G. Grün, R. Seemann, H. Mantz, K. Jacobs, K.R. Mecke, and R. Blossey. Complex dewetting scenarios captured by thin-film models. *Nature Materials*, 2(1):59–63, 2003.

[19] R. Seemann, S. Herminghaus, and K. Jacobs. Dewetting patterns and molecular forces: A reconciliation. *Physical Review Letters*, 86(24):5534–5537, 2001.

[20] W. Pechhold, O. Grassl, and W. van Soden. Dynamic shear compliance of polymer meltsand networks. In O. Güven, editor, *Crosslinking and scission in polymers*, volume 292. Springer, 1990.

[21] R. Fetzer, A. Münch, B. Wagner, M. Rauscher, and K. Jacobs. Quantifying hydrodynamic slip: A comprehensive analysis of dewetting profiles. *Langmuir*, 23(21):10559–10566, 2007.

[22] S. Herminghaus, K. Jacobs, and R. Seemann. The glass transition of thin polymer films: some questions, and a possible answer. *The European Physical Journal E: Soft Matter and Biological Physics*, 5(5):531–538, 2001.

[23] O. Bäumchen, R. Fetzer, M. Klos, M. Lessel, L. Marquant, H. Hähl, and K. Jacobs. Slippage and nanorheology of thin liquid polymer films. *Journal of Physics: Condensed Matter*, 24 (32):325102, 2012.

[24] D.W. van Krevelen. *Properties of Polymers: Their Estimation and Correlation with Chem. Structure*. Elsevier Scientific Publ., 1976.

[25] S.H. Anastasiadis, I. Gancarz, and J.T. Koberstein. Interfacial tension of immiscible polymer blends: temperature and molecular weight dependence. *Macromolecules*, 21(10): 2980–2987, 1988.

[26] S. Wu. Surface and interfacial tensions of polymer melts. II. Poly (methyl methacrylate), poly (n-butyl methacrylate), and polystyrene. *The Journal of Physical Chemistry*, 74(3): 632–638, 1970.

[27] S. Jachalski, R. Huth, G. Kitavtsev, D. Peschka, and B. Wagner. Stationary solutions of liquid two-layer thin film models. *arXiv preprint arXiv:1210.5842*, 2012.

[28] J.J. Kriegsmann and M.J. Miksis. Steady motion of a drop along a liquid interface. *SIAM Journal on Applied Mathematics*, 64(1):18–40, 2003.

[29] A. Münch and B. Wagner. Contact-line instability of dewetting thin films. *Physica D*, 209: 178–190, 2005.